The Impacts of Adjusting Momentum Roughness Length on Strong and Weak Hurricane Forecasts: A Comprehensive Analysis of Weather Simulations and Observations

MENG LI,[a] JUN A. ZHANG,[b,c] LEO MATAK,[a] AND MOSTAFA MOMEN[a]

[a] *Department of Civil and Environmental Engineering, University of Houston, Houston, Texas*
[b] *NOAA/AOML/Hurricane Research Division, Miami, Florida*
[c] *Cooperative Institute for Marine and Atmospheric Studies, University of Miami, Miami, Florida*

(Manuscript received 15 July 2022, in final form 30 January 2023)

ABSTRACT: The momentum roughness length (z_0) significantly impacts wind predictions in weather and climate models. Nevertheless, the impacts of z_0 parameterizations in different wind regimes and various model configurations on the hurricane size, intensity, and track simulations have not been thoroughly established. To bridge this knowledge gap, a comprehensive analysis of 310 simulations of 10 real hurricanes using the Weather Research and Forecasting (WRF) Model is conducted in comparison with observations. Our results show that the default z_0 parameterizations in WRF perform well for weak (category 1–2) hurricanes; however, they underestimate the intensities of strong (category 3–5) hurricanes. This finding is independent of model resolution or boundary layer schemes. The default values of z_0 in WRF agree with the observational estimates from dropsonde data in weak hurricanes while they are much larger than observations in strong hurricanes regime. Decreasing z_0 close to the values of observational estimates and theoretical hurricane intensity models in high wind regimes ($\gtrsim$45 m s^{-1}) led to significant improvements in the intensity forecasts of strong hurricanes. A momentum budget analysis dynamically explained why the reduction of z_0 (decreased surface turbulent stresses) leads to stronger simulated storms.

KEYWORDS: Hurricanes/typhoons; Numerical weather prediction/forecasting; Parameterization; Turbulence; Boundary layer; Air-sea interaction

1. Introduction

Hurricanes originate over warm tropical oceans and produce strong winds that can cause extensive damage to urban and natural environments when they make landfall (Blake et al. 2007; Kousky 2014; Cheikh and Momen 2020; Hosannah et al. 2021). The annual costs associated with hurricane damages have considerably increased in recent years (Stewart et al. 2003; Pinelli et al. 2004; Pielke et al. 2008; Bjarnadottir et al. 2011). For instance, Hurricanes Katrina (2005) and Maria (2017) together caused more than $250 billion (U.S. dollars) in adjusted costs (NOAA/NCEI 2021). Therefore, it is imperative for the scientific community to better understand and predict these extreme weather events.

To alleviate the extensive damage resulting from the increased frequency and intensity of hurricanes (Emanuel 2005, 2020), accurate and reliable forecasts from Numerical Weather Prediction (NWP) models are required. The Weather Research and Forecasting (WRF) modeling system (Skamarock et al. 2008) is a state-of-the-art NWP model that includes multiscale forecasting and data assimilation systems to predict various weather patterns. The performance of WRF in forecasting hurricane landfalls, track, and intensity has been assessed and validated by previous studies (Davis et al. 2008; Fierro et al. 2009; Abarca and Corbosiero 2011; Nasrollahi et al. 2012; Di et al. 2015; Khain et al. 2016; Romdhani et al. 2022).

Unlike high-resolution large-eddy simulations (LES; with grid spacing of ~1–100 m) that resolve turbulence (e.g., Momen and Bou-Zeid 2016; Salesky et al. 2016; Momen et al. 2018; Li et al. 2019), NWP models have to entirely parameterize turbulent fluxes due to their larger grid sizes (~1–30 km) that cannot resolve turbulence. Recent observations and LESs have shown that there are significant distinctions between hurricane turbulence and regular atmospheric boundary layer (ABL) turbulence (Zhang et al. 2009; Zhang 2010; Zhang et al. 2011, 2017; Momen et al. 2021; Chen 2022). Hence, turbulent flux parameterizations for hurricane flows need to be comprehensively examined and existing models should be exclusively tested for these unique flow systems.

One of the key elements of turbulent flux modeling is parameterizing surface momentum fluxes that are crucial in predicting hurricane intensity, structure, and track (Emanuel 1995; Moon et al. 2004; Chen et al. 2007). Since the direct measurement of the air–sea momentum flux τ is challenging, it is typically calculated using the average wind speed at 10 m U_{10} through the dimensionless drag coefficient C_d as $\tau = \rho C_d U_{10}^2$, where ρ is the air density. Previous studies have shown that C_d is not constant and depends on the surface wind speed (Miller 1964; Large and Pond 1981; Powell et al. 2003; Donelan et al. 2004; French et al. 2007; Holthuijsen et al. 2012). Since C_d

Supplemental information related to this paper is available at the Journals Online website: https://doi.org/10.1175/MWR-D-22-0191.s1.

Corresponding author: Mostafa Momen, mmomen@uh.edu

DOI: 10.1175/MWR-D-22-0191.1

affects the surface friction, it can thus modulate the force balance in the hurricane boundary layer.

The C_d values are significantly affected by the wind–wave, wave–current, and wind–wave–current interactions. Introducing the wave and ocean current effects in hurricane simulations led to remarkable changes in hurricane intensity predictions and dynamical processes (Chen et al. 2007; Warner et al. 2010; Phibbs and Toumi 2014; Katsafados et al. 2018; Mooney et al. 2019). Wave effects in these simulations considerably modulate the surface momentum roughness length (Warner et al. 2010). To resolve the ocean wave effects in hurricane simulations, the WRF atmospheric model can be coupled with the Simulating Waves Nearshore (SWAN) model. SWAN is a third-generation wave model that has been shown to provide promising results for hurricane-generated waves (Xu et al. 2007; Xie et al. 2008; Sheng et al. 2010; Dietrich et al. 2011; Huang et al. 2013). The coupling procedure has been made possible by employing the Model Coupling Toolkit (MCT) in the framework of Coupled Ocean–Atmosphere–Wave–Sediment Transport (COAWST) Modeling System (Warner et al. 2008, 2010).

Earlier studies have shown that C_d increases linearly with the surface wind speed in low to moderate wind conditions (Miller 1964; Large and Pond 1981). Despite the technical difficulties involved in the observations and laboratory studies under high wind conditions, more recent studies have shown that C_d levels off or decreases for surface wind speeds greater than ~30 m s^{-1} (Powell et al. 2003; Donelan et al. 2004; French et al. 2007; Holthuijsen et al. 2012; Curcic and Haus 2020). However, some uncertainties were found in the old and new observations among these studies (Richter et al. 2021). These discrepancies in surface layer parameterizations (e.g., C_d values for strong winds) and their impacts on the dynamics of real hurricane simulations motivate the goal of the present work.

The hurricane forecasts are significantly sensitive to both the surface flux and planetary boundary layer (PBL) parameterizations. The PBL parameterizations, which handle the transport of surface fluxes into the atmosphere at higher elevations, can substantially impact the forecasting skills of hurricane simulations (Gopalakrishnan et al. 2013; Chen et al. 2021; Gopalakrishnan et al. 2021; Hazelton et al. 2022; Chen et al. 2022). Furthermore, modifying the original formulations of C_d for each PBL scheme by limiting the surface roughness to a narrower range of values, especially at wind speeds greater than 30 m s^{-1}, which more closely matches the observations and laboratory experiments, led to stronger surface wind speeds and improved the forecasting skill of WRF (Davis et al. 2008; Nolan et al. 2009).

The surface flux parameterizations have been explored in several previous studies (Powell and Ginis 2006; Davis et al. 2008; Montgomery et al. 2011; Green and Zhang 2013, 2014; Xu et al. 2016; Lyu and Zhu 2018; Alimohammadi et al. 2020; Nellipudi et al. 2021). For example, it is found that C_d affects the pressure–wind relationship and the radius of the maximum near-surface wind using WRF simulations of Hurricane Katrina (Green and Zhang 2013, 2014). Surface turbulent fluxes including momentum, heat, and moisture fluxes used in the surface layer schemes and land surface models (LSM) are typically formulated based on the Monin–Obukhov Similarity Theory (MOST) in NWPs. Using MOST, the first model level and the ground surface are connected in WRF. The drag coefficient (C_d) in WRF is formulated as

$$C_d = \left[\frac{\kappa}{\ln(z/z_0) - \psi_m(z/L)}\right]^2, \tag{1}$$

where κ is the von Kármán constant, z_0 is the momentum roughness length, z is the height above the ground, L is the Obukhov length, and ψ_m is an empirical function that accounts for the atmospheric stability (Stull 1988; Momen 2022). The value of z_0 can be obtained from observations by fitting the logarithmic law of the wall to the measured wind profiles.

Nevertheless, our knowledge of the impacts of various z_0 parameterizations (e.g., conventional Charnock formulas) and wave-coupled models and their adjustments on weak and strong real hurricane simulations is still limited. This knowledge gap is both due to the lack of sufficient observations for strong hurricanes (compared to regular low-wind regime measurements) and, also, due to insufficient numerical and theoretical studies to characterize the applicability of current parameterizations for strong hurricane winds. For instance, to date, the impacts of different z_0 parameterizations such as in wave-coupled models on the dynamics of different hurricane regimes have not been comprehensively established. Thus, the primary objective of the current study is to bridge this knowledge gap by systematically varying the momentum roughness length within two different PBL schemes in the WRF modeling system for 10 Atlantic hurricanes ranging from category 1 to 5. We will also use the Global Positioning System (GPS) dropsondes data to estimate the measured momentum roughness length and compare that with the WRF simulation results. Improving z_0 values for strong hurricane winds (speed $\gtrsim$ 35 m s^{-1}) in surface layer parameterizations is still an active field of research due to lack of sufficient wind measurements in these extreme weather events. Considering these knowledge gaps, our research questions are as follows:

1) How do various existing surface layer parameterizations with and without hurricane wind modifications influence the track and intensity accuracy in real hurricane WRF simulations?
2) What are the impacts of increasing and decreasing the momentum roughness length for strong winds on hurricane dynamics?
3) How can we adjust the existing surface roughness parameterizations to improve the hurricane forecasting accuracy in different hurricane intensity regimes?

The paper is structured as follows. In section 2, the momentum roughness representation in WRF and the suite of conducted simulations will be described. In section 3, the numerical results as well as observations on the impacts of momentum roughness length on hurricane simulations will be shown. Questions 1, 2, and 3 will be answered in sections 3a, 3b and 3c, and 3d, respectively. Finally, the summary of the main findings will be presented in section 4.

2. Methods

a. Momentum roughness length representations in WRF

In this study, we employ the Advanced Research WRF (ARW) dynamical core to conduct hurricane simulations. ARW has been extensively used and validated in previous hurricane simulation studies (Davis et al. 2008; Fierro et al. 2009; Cavallo et al. 2013; Blake et al. 2017; Romdhani et al. 2022). WRF is a fully compressible nonhydrostatic model, that solves the Euler equations on a terrain-following, mass-based, hybrid sigma–pressure vertical coordinate. Arakawa C grid staggering is applied in the horizontal directions of the WRF Model (Skamarock et al. 2008). Please refer to online supplemental material text section S1 for more details about the WRF's governing equations.

WRF includes different z_0 parameterizations based on the PBL options. In this study, we employ and compare two widely used PBL schemes. The first scheme is Mellor–Yamada–Janjić (MYJ), which is a local turbulence closure based on turbulent kinetic energy (TKE) budget (Mellor and Yamada 1982; Janjić 1990, 1994). The surface layer z_0 for the MYJ scheme follows the Charnock formula as

$$z_0 = \mathrm{Clz}_f \times 0.0185\,\frac{u_*^2}{g}, \tag{2}$$

where u_* denotes the friction velocity, g is the gravitational acceleration, and Clz_f is a new control parameter defined in this study based on the surface wind speed to conduct sensitivity tests. In this formula, the momentum roughness length monotonically increases with increasing wind speed. For very low wind speeds, the momentum roughness length has a cutoff at a small value.

The second employed PBL scheme is the Yonsei University (YSU; Hong et al. 2006; Hong 2010), which is a nonlocal turbulence closure. There are three surface layer options for the YSU scheme. Option 0 is the default option for z_0 and its formulation is similar to the MYJ surface layer model as

$$z_0 = 0.0185\,\frac{u_*^2}{g} + \frac{0.11 \times 1.59 \times 10^{-5}}{u_*}. \tag{3}$$

Options 1 and 2 in ARW are based on Donelan's laboratory study that shows that z_0 increases with the wind speed up to ~35 m s^{-1} and then levels off for higher wind speeds (Donelan et al. 2004). Options 1 and 2 have the following formulation for z_0:

$$\begin{gathered} z_0 = \mathrm{Clz}_f[z_w z_2 + (1 - z_w)z_1], \\ z_w = \min\left\{1, \left(\frac{u_*}{1.06}\right)^{0.3}\right\}, \quad z_1 = 0.011\frac{u_*^2}{g} + 1.59 \times 10^{-5}, \\ z_2 = \frac{10}{\exp(9.5u_*^{-1/3})} + \frac{1.65 \times 10^{-6}}{\max(u_*, 0.01)}. \end{gathered} \tag{4}$$

The differences between options 1 and 2 are the heat and moisture roughness lengths, separate from momentum roughness length outlined above. In option 1, the heat and moisture roughness lengths are constant with no dependence on the wind speed, while in option 2, they are functions of z_0, u_*, Schmidt number (Sc), and Prandtl number (Pr) (Skamarock et al. 2008). Note that heat and moisture roughness lengths are not the subjects of study in this paper.

We also conduct surface wave resolving hurricane simulations by coupling WRF with SWAN. In WRF-SWAN coupled cases, z_0 is modified to consider the ocean surface wave effects by introducing the wave characteristics (Taylor and Yelland 2001; Warner et al. 2010) as

$$z_0 = \mathrm{Clz}_f\left[1200.0H_{\mathrm{wave}}\left(\frac{H_{\mathrm{wave}}}{L_{\mathrm{wave}} + 0.001}\right)^{4.5} + \frac{0.11\nu}{u_* + 0.001}\right], \tag{5}$$

where H_{wave} denotes the significant wave height, L_{wave} represents the mean wavelength, and ν denotes kinematic viscosity. The first term on the right-hand side of Eq. (5) shows the contribution of ocean waves to the surface drag and the second term represents the contribution from the surface friction.

The goal of this paper is to investigate the roughness length changes for strong winds in hurricane vortex (not the much-studied low-wind environmental flow regime). Therefore, Clz_f is defined as a piecewise function of the surface wind speed:

$$\mathrm{Clz}_f(\mathrm{wspd}_{10}) = \begin{cases} 1, & \mathrm{wspd}_{10} \le 10\,\mathrm{m\,s^{-1}}, \\ \{1 + [0.1(\mathrm{Clz} - 1)(\mathrm{wspd}_{10} - 10)]\}, & 10 < \mathrm{wspd}_{10} < 20\,\mathrm{m\,s^{-1}}, \\ \mathrm{Clz}, & \mathrm{wspd}_{10} \ge 20\,\mathrm{m\,s^{-1}}, \end{cases} \tag{6}$$

where wspd_{10} represents the 10-m wind speed. As Eq. (6) indicates, the new Clz changes will not be applied for $\mathrm{wspd}_{10} \le 10$ m s^{-1}, which represents the low-wind field that includes the environmental flow. Figure 1 depicts an example of the impact of applying this newly defined Clz parameter on surface wind intensity. A default simulation run of Hurricane Katrina (Figs. 1a,b) is compared to another run where Clz = 0.01 (Figs. 1c,d). At points where surface wind speed is greater than 20 m s^{-1}, the Clz change is in full effect, and it reduces the default z_0 to 0.01 of its unmodified value. This change leads to an increase in the intensity of the hurricane (cf. Figs. 1b,d) that will be extensively discussed in the next sections. We note that the primary objective of this study is to determine the accuracy of current z_0 parameterizations for high wind regimes by conducting a comprehensive sensitivity test according to the above formulation. Optimizing the values of z_0 for different

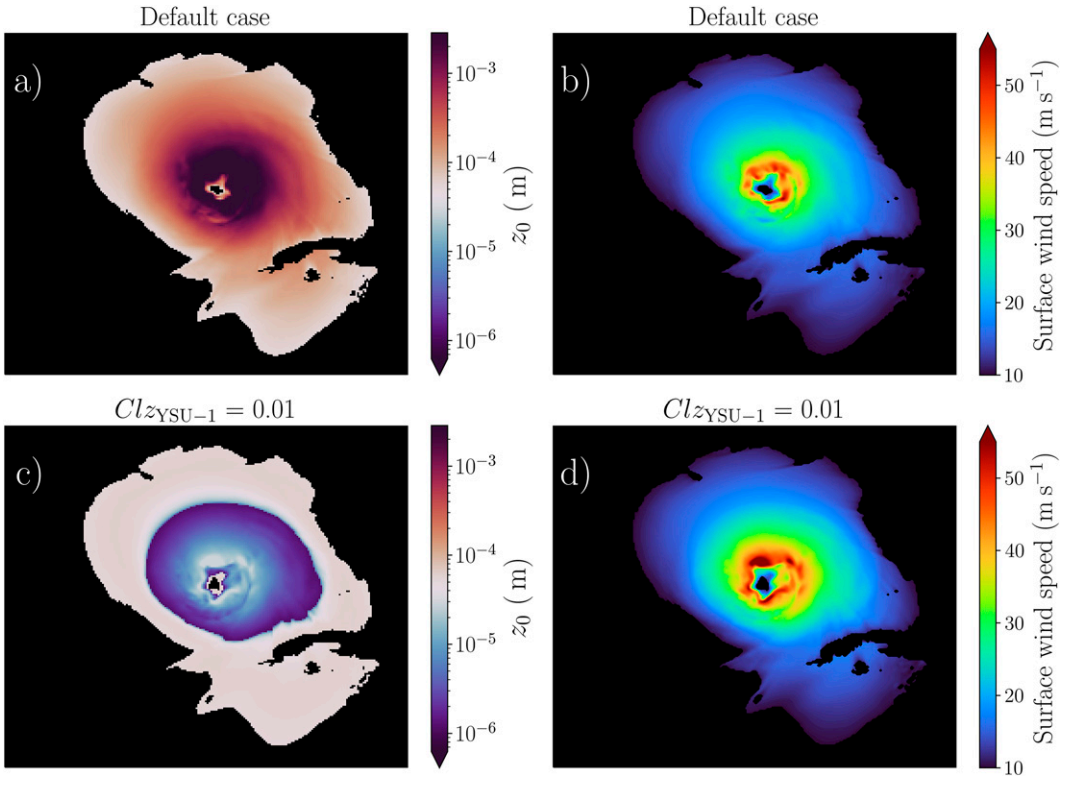

FIG. 1. Implementation of the Clz_f coefficient to the surface roughness z_0 based on the surface wind speed (Hurricane Katrina simulation). Logarithmic contours of z_0 for (a) the default and (c) the reduced roughness length case. The surface wind speed contours for (b) the default and (d) the reduced roughness length case.

wind regimes will be done in future work based on a thorough comparison with observations.

b. *Suite of simulations*

To investigate the impacts of different z_0 parameterizations on real hurricane forecast accuracy, 10 Atlantic Hurricanes were simulated. The chosen hurricane cases are divided into two groups: the strong hurricane group and the weak hurricane group. Hurricanes Katrina (2005), Igor (2010), Maria (2017), Dorian (2019), and Lorenzo (2019) are category 3–5 based on the Saffir–Simpson hurricane wind scale (Simpson and Saffir 1974; Taylor et al. 2010) and are thus referred to as strong hurricanes in this study. During the simulated periods, the maximum observed surface wind speeds for these five major hurricanes are 77, 67, 57, 82, and 67 m s^{-1}, respectively. Category-1–2 hurricanes are considered weak hurricanes. Hurricanes Ike (2008), Cristobal (2014), Joaquin (2015), Nicole (2016), and Gert (2017) are selected as weak hurricanes for which their maximum surface wind speeds are 44, 36, 44, 44, and 46 m s^{-1}, respectively.

All the initial fields of the simulations come from the Global Forecast System (GFS) for National Centers for Environmental Prediction (NCEP/NWS/NOAA/U.S. Department of Commerce 2015). Only one initial time is considered for each hurricane case. The start date of each case is different depending on the genesis of each hurricane, and each simulation is conducted for 30–48 h. The simulation periods were chosen considering two factors: first the strong hurricanes stay category 3–5 and weak hurricanes remain category 1–2 during the entire simulation period, and second the hurricanes stay over the Ocean and do not make landfall during the simulations.

In total, 310 simulations were conducted to examine the parameter space of the problem by varying the PBL schemes, surface flux options, z_0 parameterizations, and grid resolution. Table 1 summarizes the suite of conducted simulations that took more than 2 million CPU-hours and 20 TB of disk space. Four sets of WRF-only simulations and one set of WRF-SWAN coupled simulations (WRF-COAWST) are conducted. For the WRF-only cases, two employed PBL schemes are MYJ and YSU. For the YSU scheme, three surface flux options are selected according to Eqs. (3) and (4). The WRF-SWAN coupled simulation in the COAWST framework is also conducted to explicitly consider the ocean surface wave effects. More details about the WRF, SWAN model, and simulation setups can be found in supplemental material S1. In section 3a, the cases using the original z_0 models (referred to as the default cases hereafter) for the 10 considered hurricanes will be presented. In sections 3b and 3d, the default z_0 is modified using the newly added control parameter Clz in Eqs. (2), (4), and (5) from 10^{-4} to 10^{2} to characterize the sensitivity of the hurricane simulations to momentum roughness length. Note that these large changes of z_0 translate into much

TABLE 1. Numerical simulations conducted for the sensitivity study of the momentum roughness length using WRF only and WRF-SWAN coupled models with different grid sizes. Here placeholder **X** denotes the considered grid resolutions. We conducted 8- and 32-km simulations for all hurricanes and models, while 2-km simulations, due to their expensive computational costs, are only carried out for WRF-YSU-1 with Clz = 0.01, 1, and 100. The next placeholder **Y** denotes the values of the control parameter Clz that can be 0.0001, 0.01, 1, or 100. For example, Ka_2km_YSU1_Clz100 represents the simulation of Hurricane Katrina using the WRF Model with the YSU PBL scheme, for which the surface flux option is 1, the grid size is 2 km, and the order of magnitude of the roughness is increased by a factor of 2. For WRF-YSU-0 and WRF-MYJ, only default Clz is simulated. In total, we conducted $2 \times 2 \times 10 + 3 \times 2 \times 10 \times 4 + 3 \times 10 = 310$ simulations.

Hurricane	WRF-YSU-0	WRF-YSU-1	WRF-YSU-2	WRF-MYJ	WRF-COAWST
Katrina	Ka_**X**km_YSU0	Ka_**X**km_YSU1_Clz**Y**	Ka_**X**km_YSU2_Clz**Y**	Ka_**X**km_MYJ	Ka_**X**km_COAWST_Clz**Y**
Igor	Ig_**X**km_YSU0	Ig_**X**km_YSU1_Clz**Y**	Ig_**X**km_YSU2_Clz**Y**	Ig_**X**km_MYJ	Ig_**X**km_COAWST_Clz**Y**
Maria	Ma_**X**km_YSU0	Ma_**X**km_YSU1_Clz**Y**	Ma_**X**km_YSU2_Clz**Y**	Ma_**X**km_MYJ	Ma_**X**km_COAWST_Clz**Y**
Dorian	Do_**X**km_YSU0	Do_**X**km_YSU1_Clz**Y**	Do_**X**km_YSU2_Clz**Y**	Do_**X**km_MYJ	Do_**X**km_COAWST_Clz**Y**
Lorenzo	Lo_**X**km_YSU0	Lo_**X**km_YSU1_Clz**Y**	Lo_**X**km_YSU2_Clz**Y**	Lo_**X**km_MYJ	Lo_**X**km_COAWST_Clz**Y**
Ike	Ik_**X**km_YSU0	Ik_**X**km_YSU1_Clz**Y**	Ik_**X**km_YSU2_Clz**Y**	Ik_**X**km_MYJ	Ik_**X**km_COAWST_Clz**Y**
Cristobal	Cr_**X**km_YSU0	Cr_**X**km_YSU1_Clz**Y**	Cr_**X**km_YSU2_Clz**Y**	Cr_**X**km_MYJ	Cr_**X**km_COAWST_Clz**Y**
Joaquin	Jo_**X**km_YSU0	Jo_**X**km_YSU1_Clz**Y**	Jo_**X**km_YSU2_Clz**Y**	Jo_**X**km_MYJ	Jo_**X**km_COAWST_Clz**Y**
Nicole	Ni_**X**km_YSU0	Ni_**X**km_YSU1_Clz**Y**	Ni_**X**km_YSU2_Clz**Y**	Ni_**X**km_MYJ	Ni_**X**km_COAWST_Clz**Y**
Gert	Ge_**X**km_YSU0	Ge_**X**km_YSU1_Clz**Y**	Ge_**X**km_YSU2_Clz**Y**	Ge_**X**km_MYJ	Ge_**X**km_COAWST_Clz**Y**

smaller changes in the default friction velocity (~0.5–2 times the default value) due to the logarithmic relationship of z_0 with u_*.

c. Evaluation metrics

In this study, we evaluate the performance of the simulations by calculating the mean absolute error (MAE) for the hurricane track and mean absolute percentage error (MAPE) for the surface wind intensity, compared to the observations. To this end, the U.S. National Hurricane Center (NHC) best track and intensities reported data are used. Generally, different weather and climate models with various weights (Kidder et al. 2000; Klotz and Uhlhorn 2014; Huffman et al. 2015) are employed to conduct the NHC forecasts. The MAE is formulated as

$$\mathrm{MAE}_{\mathrm{Track}} = \frac{1}{N}\sum_{i=1}^{N} |F_{\mathrm{Track}}(t_i) - O_{\mathrm{Track}}(t_i)|, \tag{7}$$

where N is the total sample number, and $F_{\mathrm{Track}}(t_i)$ denotes the forecasted location of the hurricane eye at time t_i, based on the minimum sea level pressure, and $O_{\mathrm{Track}}(t_i)$ represents the best-observed hurricane eye location at time t_i. For track, MAE is calculated in terms of distance in km. The sampling time interval is based on the interval time of the reported best track data ($t_{i+1} - t_i = 6$ h).

For the storm intensity error calculation, we define a separate MAE similar to Eq. (7) in which $F_{\mathrm{Intensity}}(t_i)$ and $O_{\mathrm{Intensity}}(t_i)$ represent the maximum forecasted and observed 10-m wind speed intensities at time t_i, respectively. Furthermore, to better compare the forecasting accuracy of the wind intensity in different weak and strong wind regimes, we normalize the $\mathrm{MAE}_{\mathrm{Intensity}}$ with the observed wind data to obtain the MAPE for each case (Romdhani et al. 2022) as

$$\mathrm{MAPE}_{\mathrm{Intensity}} = \frac{1}{N}\sum_{i=1}^{N} \left| \frac{F_{\mathrm{Intensity}}(t_i) - O_{\mathrm{Intensity}}(t_i)}{O_{\mathrm{Intensity}}(t_i)} \right| \times 100\%. \tag{8}$$

3. Results and discussions

a. Track and intensity errors in simulations with the default setup of roughness length

First, the performance of the default surface options is evaluated. To quantitatively analyze the accuracy of the hurricane track and intensity forecasts, the normalized 10-m wind intensity and absolute hurricane track errors are calculated. The wind intensity time series and hurricane tracks (see supplemental material S2 and S3) are employed to calculate the errors in Eqs. (7) and (8). The averaged MAE among these hurricanes simulations is depicted in Fig. 2 for the default z_0 parameterizations.

In the WRF-COAWST model, the employed PBL scheme is MYJ. As can be seen in Fig. 2, including the ocean wave effects (dark blue bars) in the considered cases improves the intensity predictions by ~7% and track by ~8% compared to the default MYJ scheme (green bars). Among all the employed models, the YSU scheme's option 1 appears to have the best performance for predicting wind intensities in the considered cases by reducing option 0's $\mathrm{MAPE}_{\mathrm{Intensity}}$ by ~5%. A similar result was found when comparing the mean absolute error of the intensity forecasts (see Fig. S9 in the supplemental material). YSU-1 had the lowest MAE error of ~10 m s^{-1} compared to the MYJ scheme which had the highest MAE intensity error of ~12 m s^{-1}. Furthermore, Fig. 2a shows that the simulations with the YSU scheme, which is the recommended PBL scheme by the ARW's guideline for hurricane simulations (Wei et al. 2019), relatively outperform the MYJ's hurricane intensity forecasts. In terms of track error, WRF-COAWST has the best performance among the considered models.

b. Impacts of changing the momentum roughness length on hurricane forecasts

The momentum roughness length can significantly impact the intensity, structure, and size of the simulated hurricanes.

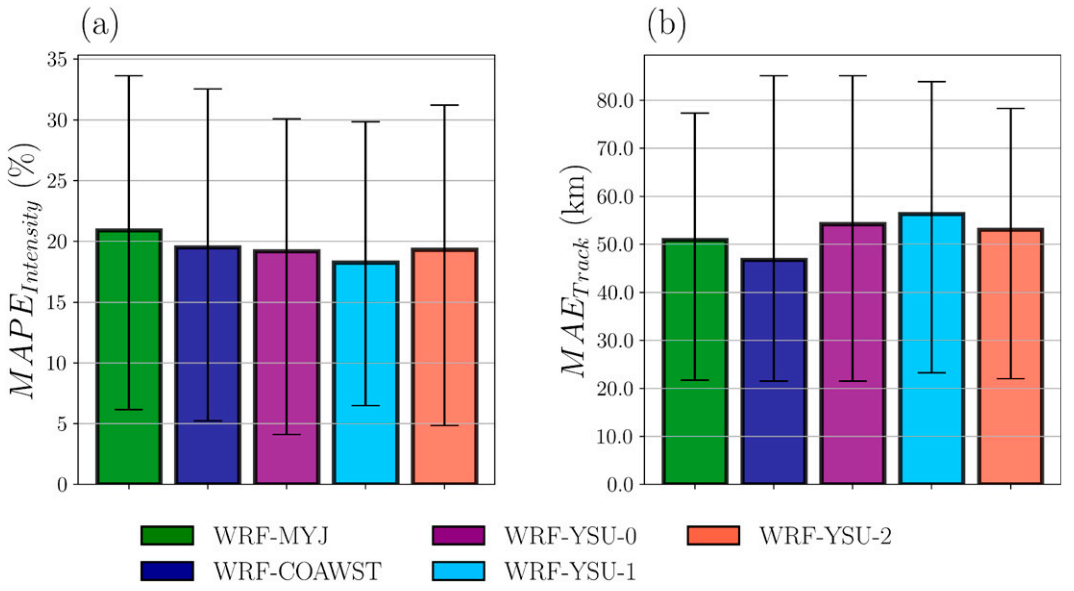

FIG. 2. Overview of the simulated results for hurricane intensity and track forecasts from different models using their default momentum roughness lengths with 8-km grid spacing: (a) the normalized 10-m wind intensity errors and (b) the track errors. The error bars show the range from the 20th percentile to the 80th percentile of the errors. In total, 450 samples from 50 simulations (10 hurricanes × 5 models) were used in this figure.

To characterize these effects, we explicitly adjusted z_0 in WRF. Figure 3 depicts the maximum 10-m wind speed time series of the five strong hurricanes using the WRF-YSU-1 model with various Clz. As can be seen from Figs. 3a–e, the simulations using the default z_0 (Clz = 1) underestimate the observed storm intensity in strong hurricanes. Decreasing the magnitude of z_0 intensifies the hurricanes and increases the maximum surface wind speed (see blue and gray lines in Fig. 3) and vice versa. Based on an initial qualitative observation from this figure, for the strong hurricane cases presented in this paper, decreasing z_0 generally improves the accuracy of the surface wind intensity predictions. A more comprehensive quantitative analysis of the impacts of changing the default z_0 on the accuracy of simulated hurricanes will be presented in section 3d.

Altering z_0 values also impact the size and structure of the hurricanes. The wind speed at 10-m altitude is illustrated in Fig. 4 for each hurricane. By decreasing z_0, the storm size increases compared to the default case (see orange areas in Fig. 4). Moreover, consistent with the comparisons of time series of wind

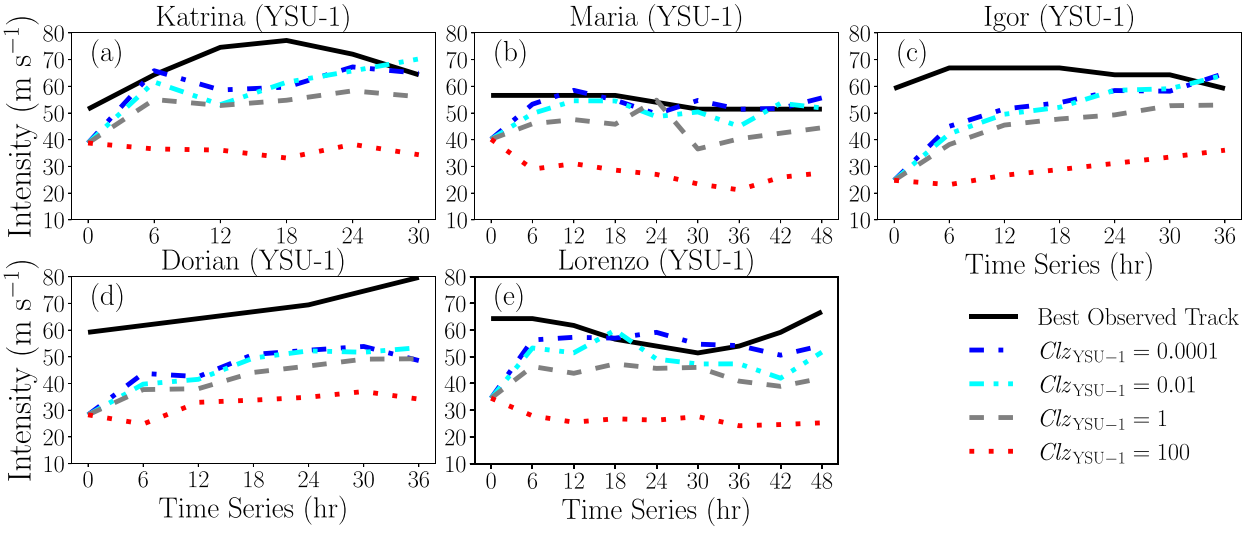

FIG. 3. The sensitivity study of the WRF-YSU-1 model by changing the control parameter Clz with 8-km grid spacing, showing the storm intensity in comparison with the best observed track speed for five strong hurricanes.

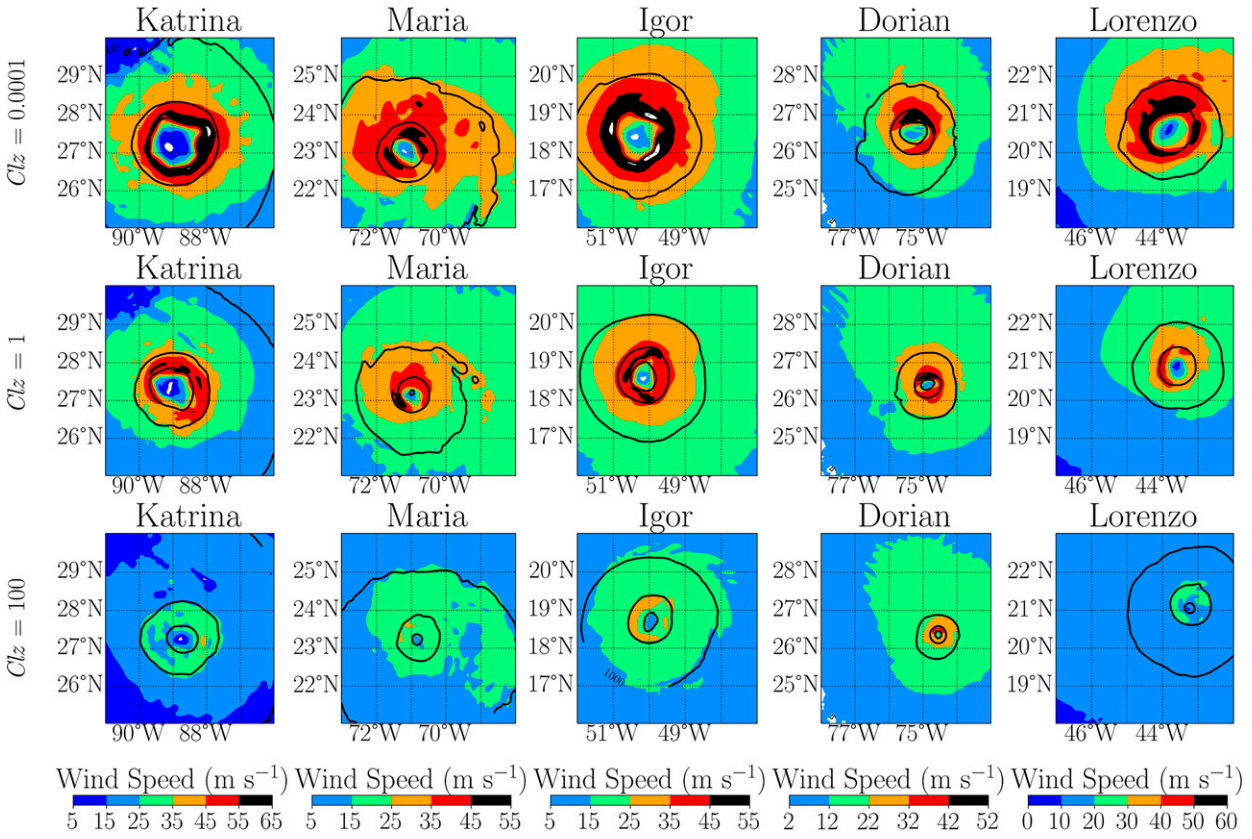

FIG. 4. Horizontal view of 10-m wind speed contours (colors) for five hurricanes with three different momentum roughness lengths at 24 h of simulation. The black lines represent isobars.

intensity, Fig. 4 indicates that a smaller z_0 results in a larger maximum wind speed (cf. black color contours in Fig. 4). Nevertheless, the radius of the maximum wind does not appear to significantly change with decreasing z_0 (see supplemental material S6 for more details).

Changing the surface roughness length can also impact the asymmetry of hurricanes. By calculating the averaged variance of the surface wind speed at each radius through the coefficient of variance (CV; not shown), we found that CV $\sim$ 12% for Clz = 100 cases and CV $\sim$ 24% for Clz = 0.0001 cases on average. This implies that decreasing z_0 increased the deviations from the mean wind value which in turn increased the asymmetry of the considered hurricanes. This can be because decreasing z_0 increases the strength of the overall wind field which can enhance instabilities in the flow while increasing z_0 (surface friction) suppresses the development of strong instabilities. Thus, decreasing z_0 can have significant implications for low-level wind asymmetry which can lead to stronger wind gusts in hurricanes.

The vertical wind speed profiles are also influenced by changes in the momentum roughness length. Decreasing z_0 intensifies the averaged tangential wind speed in the boundary layer in the hurricane eyewall region (see supplemental material S7). Figure 5 depicts the radius–height distribution of the wind speed for the default cases (Clz = 1) in comparison with the Clz = 0.0001 and Clz = 100 cases. As clearly shown in Fig. 5, the wind speed in the hurricane eyewall region is remarkably increased for Clz = 0.0001 cases (more red colors), while the wind speed is greatly decreased by increasing z_0. We also noticed that the radial inflow layer depth decreases with decreasing the surface roughness leading to a more intense hurricane and vice versa (not shown). Similar results were found for other employed models (YSU-2 and COAWST) and other grid resolutions, indicating the generality of these findings. Note that the sensitivity analysis of z_0 for other grid sizes and models can be found in supplemental material S2–S4. The impacts of z_0 changes on hurricane track will be presented in section 3d.

c. *Physical explanation of the effects of momentum roughness length on hurricane intensity*

To shed light on the dynamical effects of the momentum roughness length on hurricane intensity forecasts, the momentum budget is analyzed using a simple single-column model of hurricanes described in Bryan et al. (2017). Following Momen et al. (2021) and assuming the gradient transport theory for turbulent fluxes [aka K theory; see (Stull 1988; Momen 2022)], the momentum equations in radial and tangential directions in the hurricane boundary layer (HBL) can be written as

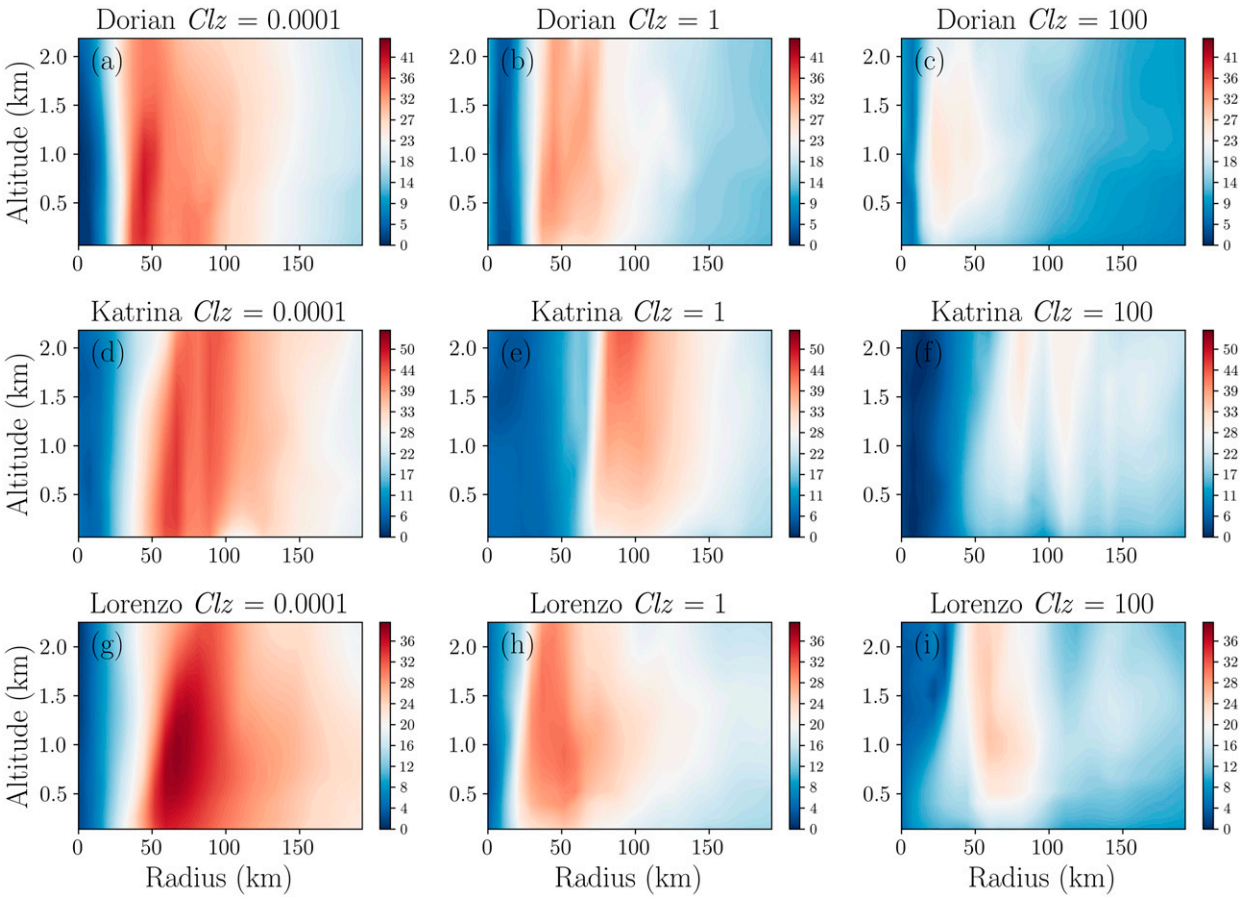

FIG. 5. Radius–height distribution of the azimuthally averaged wind speed (m s^{-1}) for Hurricanes (top) Dorian, (middle) Katrina, and (bottom) Lorenzo with three different roughness lengths at 30 h of simulation.

$$\frac{\partial u_r}{\partial t} = \left(-fV_g - \frac{V_g^2}{R}\right) + fu_\theta + \frac{u_r^2}{R} + \frac{u_\theta^2}{R} + \frac{1}{\rho}\frac{\partial}{\partial z}\left(-\nu_T \frac{\partial u_r}{\partial z}\right), \tag{9}$$

$$\frac{\partial u_\theta}{\partial t} = -fu_r - u_r \frac{\partial V_g}{\partial R} - \frac{u_\theta u_r}{R} + \frac{1}{\rho}\frac{\partial}{\partial z}\left(-\nu_T \frac{\partial u_\theta}{\partial z}\right), \tag{10}$$

where u_θ and u_r are tangential and radial velocity, and f denotes the Coriolis frequency (5×10^{-5} s^{-1} here), and ν_T is the eddy viscosity. For the eddy viscosity $\nu_T(z)$, we employed a similar profile to O'Brien's profile (O'Brien 1970). Using this analytical eddy viscosity profile formula, we can close Eqs. (9) and (10) and solve the governing partial differential equations numerically. The gradient wind velocity profile V_g at a distance R (=40 km here) from the hurricane center is set to 60 m s^{-1} at the surface and gradually decrease it to 0 m s^{-1} at 20-km height similar to Bryan et al. (2017). Finally, $\partial V_g/\partial R$ represents the radial gradient of this velocity profile, which we set to -0.33×10^{-2} s^{-1} following Momen et al. (2021).

The second term in the rhs of Eq. (9) and the first term in the rhs of Eq. (10) are the Coriolis acceleration, and the last terms denote the turbulent stresses. The first term in the bracket on the rhs of Eq. (9) represents the pressure-gradient acceleration [$(1/\rho)(\partial p/\partial r) = -fV_g - V_g{}^2/R$], the third term denotes the radial advection, and the fourth term shows the centrifugal acceleration. Similarly, for the tangential velocity, the second term and third term in the rhs of Eq. (10) represent the radial advection and centrifugal acceleration, respectively.

Near the surface, the eddy viscosity profile can be approximated as $\nu_T \sim \kappa u_* z$. Given the imposed eddy viscosity profile, the surface friction velocity u_* can be estimated. Next, the logarithmic wind law can be used to provide a bottom Dirichlet boundary condition for the wind speed at the first vertical node above the surface as $U(z) = u_*/\kappa \ln(z/z_0)$. The z_0 values are then varied to characterize their impacts on hurricane wind profiles. The default z_0 is set to 2×10^{-4} m. To investigate the physical mechanisms subject to varying z_0, we consider three cases with Clz = 0.0001, 1, and 100. Figure 6 shows the vertical profiles of the wind velocity, and the momentum budget terms. Compared with the default case (Clz = 1, $z_0 = 2 \times 10^{-4}$ m), ~80% increase in magnitude on u_θ is found near the surface when the z_0 is decreased (Fig. 6a). When increasing z_0, the surface friction and thus the inflow depth and magnitude are expected to increase, which is confirmed in Fig. 6a that shows that the magnitude of u_r (dashed red line) increases with z_0.

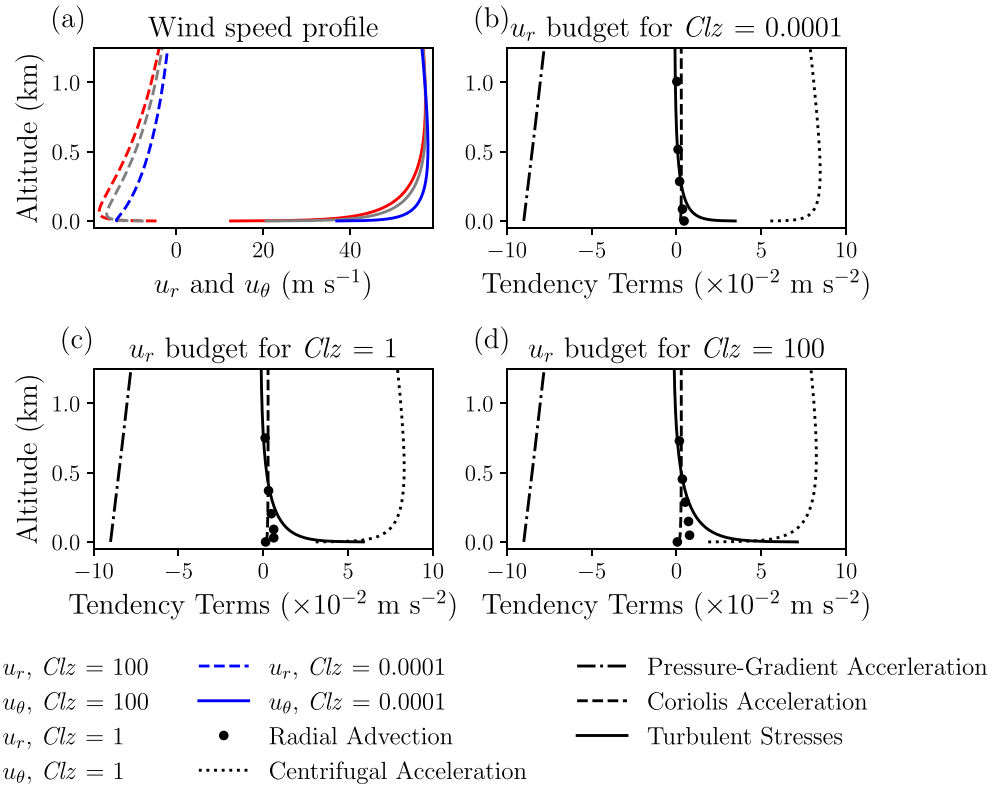

FIG. 6. Profiles of (a) tangential and radial velocity and (b)–(d) their momentum budget terms from the single-column model results with three different momentum roughness lengths.

This behavior of u_θ and u_r can be explained by assessing the momentum budget terms. The radial momentum budget terms in Eq. (9) are depicted in Figs. 6b–d assuming a quasi-steady state ($\partial u_r/\partial t \approx 0$). When decreasing z_0, the surface turbulent stress (solid line in Figs. 6b–d) decreases. For a given pressure-gradient acceleration $[(1/\rho)(\partial p/\partial r) = -fV_g - V_g^2/R]$, the centrifugal ($u_\theta^2/R$) and Coriolis ($fu_\theta$) accelerations must increase near the surface to compensate for the reduction in the turbulent stress $[(1/\rho)(\partial/\partial z)(-\nu_T \partial u_r/\partial z)]$. This indicates that the hurricane tends to intensify especially near the surface after decreasing z_0 and vice versa. Hence, altering z_0 modifies the momentum balance near the surface by modulating the turbulent stresses and can thus change the wind intensity in hurricanes. As can be seen from Fig. 6a, the impact of this surface intensification continues above the surface up to ~1000 m. Hence, most of hurricane intensification caused by the surface roughness length modifications is expected to occur within the HBL, and the free atmosphere is not expected to be significantly impacted by the surface layer changes.

d. *The impacts of varying momentum roughness length on the accuracy of strong and weak hurricanes forecasts*

In this section, we characterize the impacts of adjusting z_0 on the accuracy of real hurricane simulations and investigate the validity of existing models under different wind regimes. Modifying the momentum roughness length also influences the simulated hurricane tracks. Figure 7 displays the simulated hurricane tracks for the YSU-1 model under four different values of Clz. Decreasing z_0 (cyan and blue lines) improved the track forecasts for most hurricanes, whereas for some a modestly worsened track prediction was found. Nonetheless, a slight overall improvement of the track forecasts in decreased z_0 cases can be seen in Fig. 7, when compared to the default case (gray line), in the considered strong hurricane cases. This improvement further shows that WRF likely overestimates the actual z_0 in strong hurricane winds as decreasing it improves both track and intensity forecasts of the simulated strong hurricanes.

To comprehensively assess the hypothesis that WRF overestimates z_0 in strong hurricanes, we calculated the $\text{MAPE}_{\text{Intensity}}$ and $\text{MAE}_{\text{Track}}$ forecasts for all WRF-COAWST, WRF-YSU-1, and WRF-YSU-2 simulations. We also separated the cases into weak and strong hurricanes to determine whether the same conclusion can be drawn for weak hurricanes. The overall statistics of the $\text{MAPE}_{\text{Intensity}}$ and $\text{MAE}_{\text{Track}}$ for both category-1–2 and category-3–5 hurricanes with various imposed z_0 values are shown in Fig. 8. Increasing z_0 (red bars in Fig. 8) consistently exacerbates the intensity and track prediction issues compared to the default values (gray bars in Fig. 8). Of note, even though similar trends are observed for all three models, there are some distinctions in the degree of sensitivity among them. For example, in Fig. 8a, more than 92% increase in $\text{MAPE}_{\text{Intensity}}$ (29% absolute change) is observed when increasing z_0 from its default

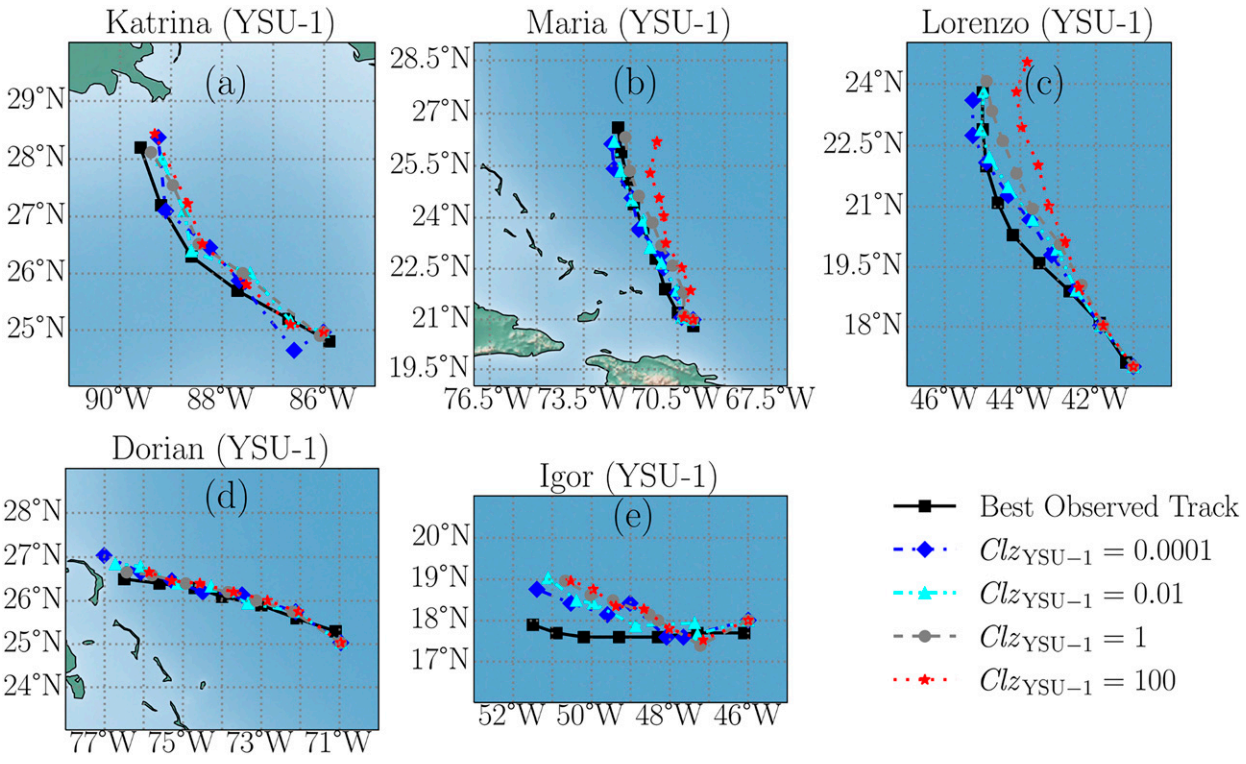

FIG. 7. Hurricane tracks for different momentum roughness lengths using 8-km grid spacing for strong hurricane (category-3–5) cases.

value (cf. gray and red bars) for WRF-YSU-2, while only ~27% increase in $MAPE_{Intensity}$ (8% absolute change) is obtained for WRF-COAWST.

As can be seen from Fig. 8a, hurricane intensity predictions are improved among all the three considered models by decreasing z_0 in category-3–5 hurricanes. The intensity improvements by decreasing z_0 (cyan bars) for COAWST, YSU-1, and YSU-2 compared to the default models (gray bars) are, respectively, about 12%, 27%, and 31%. Figure 8b indicates that the track forecasts are also slightly improved when z_0 is decreased. This improvement is about 7% for COAWST, 18% for YSU-1, and 12% for YSU-2 when comparing cyan (decreased z_0) and gray (default cases) bars in Fig. 8b. For further decreasing the z_0 values (dark blue bars) compared to the default cases (gray bars), the forecasting improvement becomes ~32% for intensity and ~6% for track on average for the three considered models. Hence, these results confirm that the default z_0 in the WRF Model most likely overpredicts the actual z_0 in the considered strong hurricanes.

Previous studies have shown that the intensity of simulated storms is sensitive to the ratio of the enthalpy (C_k) and momentum (C_d) surface exchange coefficients, C_k/C_d. The maximum potential intensity (MPI) of a given storm increases with the increase of this ratio (Emanuel 1988). In the high wind regions of intense storms, the ratio most likely lies in the range of 1.2–1.5 (Emanuel 1995). Nevertheless, the general surface flux schemes in WRF typically result in a ratio of less than 1 (Green and Zhang 2013; Alimohammadi et al. 2020). In the current study, the mean C_k/C_d ratio for the considered Clz = 0.0001, 0.01, 1, and 100 YSU-1 cases are 1.7 ± 0.1, 1.2 ± 0.1, 0.8 ± 0.1, and 0.3 ± 0.04, respectively. Thus, Clz = 0.0001 and 0.01 scenarios raise the C_k/C_d ratio to more than 1.2 compared to the default case (0.8 ± 0.1) that is consistent with the high wind region range of intense storms in prior theoretical studies (Emanuel 1995). Our result shows that the storm intensity is smaller when z_0 is increased, consistent with the MPI theory. This linkage between storm intensity and the C_k/C_d ratio provides further physical insight into the observed intensity forecast improvements in reduced z_0 strong hurricane simulations in addition to the radial momentum budget discussion in section 3c.

To determine whether decreasing the default z_0 improves the track and intensity accuracy of category-1–2 hurricanes, we also simulated five weak hurricanes as mentioned in section 2b. Figures 8c and 8d shows that unlike strong hurricanes, decreasing z_0 in weak hurricanes does not necessarily improve the intensity and track predictions. In fact, the default z_0 simulations outperform other cases, indicating that the default z_0 models likely have the optimum values for the considered category-1–2 hurricanes. Furthermore, another suite of simulations for three tropical storms [Sebastien, Gabrielle, and Jerry (not shown)] yielded a finding akin to the considered weak hurricanes. Note that similar results to Fig. 8 were found for simulations with different grid spacings demonstrating that our findings are robust and independent of model resolution. The statistics for all simulations with different grid resolutions are reported in supplemental S4, showing that the existing z_0 parameterizations in WRF are suitable for

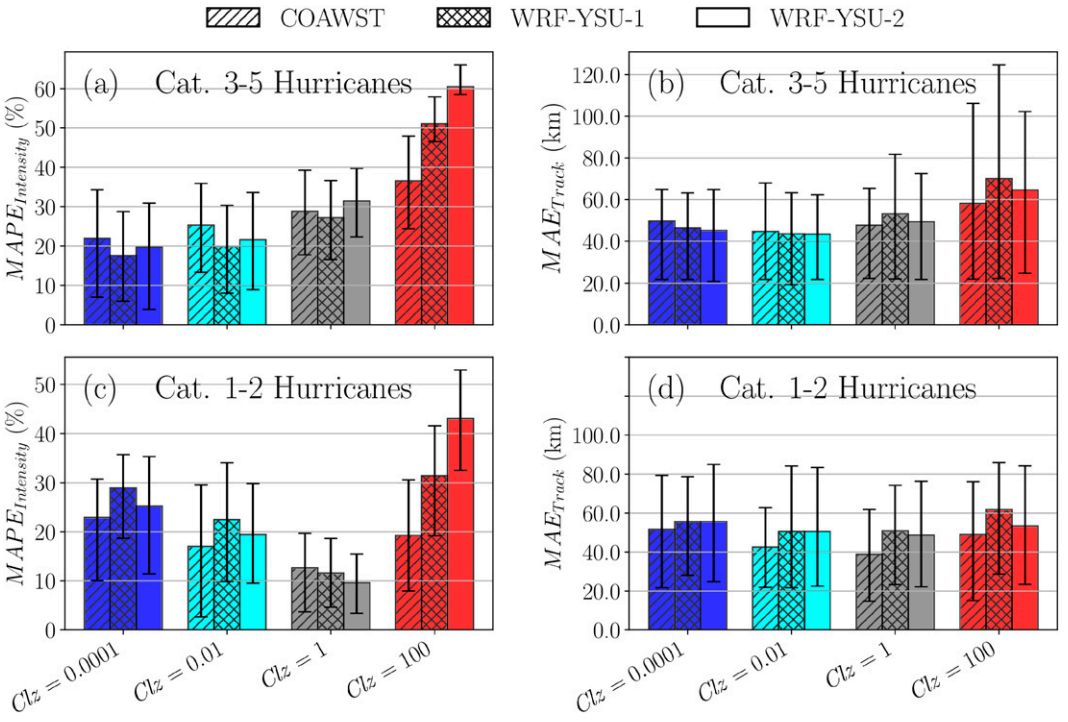

FIG. 8. Hurricane intensity and track errors with various momentum roughness lengths using 8-km grid spacing. The error bars show the range from the 20th percentile to the 80th percentile.

forecasting weak hurricane cases; however, the current z_0 parameterizations need improvements for accurate strong hurricane forecasts.

e. *Comparing z_0 values in WRF with observational estimates*

Our results indicate that while the current WRF z_0 parameterizations perform well in weak hurricanes, they lead to lower predicted intensities in strong hurricanes. For example, Fig. 9a shows the comparison between the forecasted intensities of Hurricane Maria (2017), which is a major hurricane. It is evident that the default z_0 case (gray line) underestimates the intensity compared with the observations, while the cases with smaller z_0 values (blue and cyan lines) better agree with the observed intensities. Nevertheless, as can be seen from Fig. 9b, the default z_0 setup for weak Hurricane Cristobal (2014) has the best performance, while other cases with different z_0 parameterizations either overestimate or underestimate the intensity.

To better understand why the default z_0 cases underestimate the hurricane intensity for strong hurricanes, we directly compared the z_0 values in WRF against observational estimates. We analyzed wind data from 852 dropsondes collected in Hurricanes Katrina, Maria, Lorenzo, Joaquin, Ike, Igor, Dorian, and Cristobal. Then, the vertical profiles of wind for every 10 m s^{-1} bin were selected and the corresponding u_* and z_0 for each bin was calculated by fitting the log law to the averaged wind speed profile in each bin following (Powell et al. 2003; Holthuijsen et al. 2012). Further details about the dropsondes data and the fitting procedures to evaluate z_0 from the observed GPS data can be found in Fig. S12 in the supplemental material. The results of z_0 from observations are shown in Figs. 9c–e as black lines. As the surface wind increases, the observed z_0 first increases to a maximum value of ~0.01 m at $U_{10} \sim 38$ m s^{-1}, then it slightly decreases as U_{10} further increases. Note that the fact that z_0 does not vary monotonically as a function of U_{10} has been reported in previous studies as well (e.g., Powell et al. 2003; Donelan et al. 2004; French et al. 2007). This result suggests that the surface flow characteristics in low–moderate wind regimes are different from those in high wind regimes likely due to different sea state and sea-spray distributions (Andreas and Emanuel 2001; Emanuel 2003; Moon et al. 2004; Chen et al. 2013).

WRF's z_0 for different hurricane intensities and model setups are also depicted in Figs. 9c–e for comparison purposes. The mean observed intensities for the considered strong and weak hurricanes are denoted by the purple and green vertical lines, respectively. The green and purple shadows show the standard deviations of the observed intensities for strong and weak hurricanes, respectively. The changes in z_0 are not applied for wind speeds lower than 10 m s^{-1} and, hence, the z_0 values of all cases collapse for such low surface winds in Fig. 9 as expected. It is evident that the default z_0 values in all three models (gray lines) agree with the dropsondes observations (black lines) for weak hurricanes; however, WRF's default z_0 values are much larger than the observations for strong hurricanes. The z_0 values in Clz = 0.01 cases (cyan lines) agree better with the observations for strong hurricanes than other

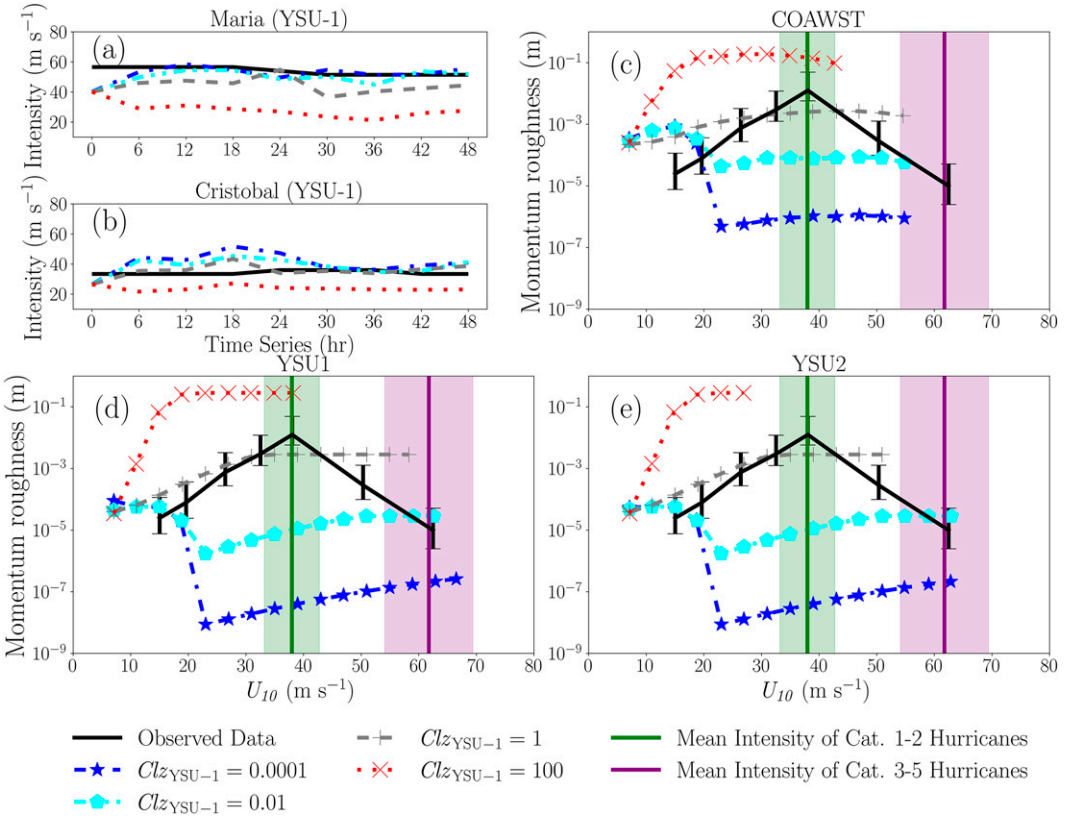

FIG. 9. Comparison of the momentum roughness lengths between observed data and the forecasted data. The forecasted wind intensity time series for Hurricanes (a) Maria (2017) and (b) Cristobal (2014). (c)–(e) The observed data from GPS dropsondes. The forecasted momentum roughness lengths for the three models are also shown in (c)–(e). The green vertical lines represent the mean observed intensity of the category-1–2 hurricanes, and the green shadows display their standard deviations. The purple counterpart represents the mean and standard deviations of the category-3–5 hurricanes.

z_0 parameterizations. Our results shown earlier indicated that these Clz = 0.01 cases outperform the default z_0 cases in terms of intensity and track forecasts of strong hurricanes.

To better illustrate these findings in terms of z_0 comparisons, we compared the WRF's forecasted vertical profiles of wind versus the dropsonde data in two mean U_{10} ranges, ~40 versus ~60 m s^{-1}, to represent weak and strong hurricanes (Fig. 10). Here, we used the default z_0 parameterization in YSU-1 from Eq. (4) and calculated a logarithmic wind profile near the surface. For the 40 m s^{-1} group, the simulated wind profiles based on the default WRF z_0 parameterization agree quite well with the observations. However, for the 60 m s^{-1} group, the default WRF z_0 parameterization considerably underestimates the wind speed in the surface layer, consistent with the results in storm intensity comparisons shown earlier.

These comparisons demonstrate that while current z_0 parameterizations in the WRF system perform well for weak hurricanes, they significantly overestimate the observed z_0 in stronger wind regimes. The z_0 comparison also helps explain why decreasing z_0 by a certain degree led to improved intensity forecasts in the considered strong hurricanes. The larger values of modeled roughness lengths in strong hurricanes may hinder the capability of WRF to accurately simulate strong hurricanes (categories 3–5) and thus the reduction of the existing momentum roughness length parameters in high wind regimes is recommended.

To implement these z_0 changes in operational models, we suggest adjusting the current z_0 estimations based on a comprehensive comparison with a wide range of different hurricane observations. These adjustments can be implemented either by changing the empirical model coefficients (e.g., in wave-coupled simulations), by altering the model structure, or by adding an observation-optimized factor for strong winds. In general, careful z_0-adjustments for strong winds are recommended using measurements and ensemble NWP simulations of many storms in operational models. The goal of this paper was to show this deficiency for strong winds in the current surface roughness parameterizations of WRF and provide some guidance on adjusting the current z_0 values that can remarkably improve hurricane forecasts.

4. Conclusions

The current study characterizes the impacts of different surface flux parameterizations on the accuracy of forecasting real

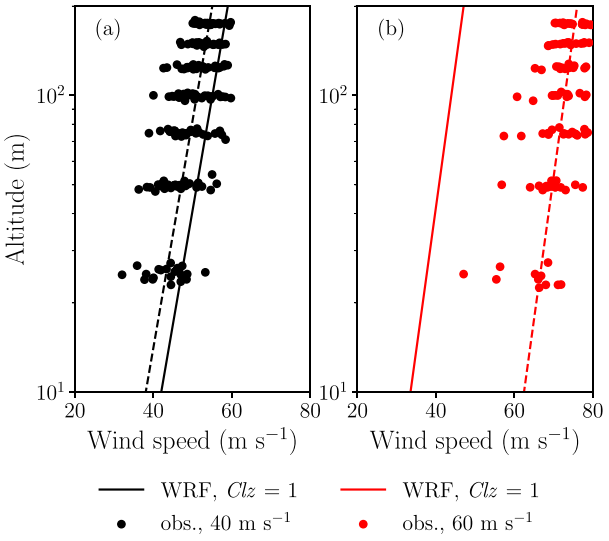

FIG. 10. Comparison of wind speed profiles between observed and forecasted data. The observed data with the 10-m wind speed of around (a) 40 and (b) 60 m s^{-1} are plotted using dots. The mean observed wind profiles are represented as dashed lines. The solid lines show the wind speed profiles obtained using the default momentum roughness length of the WRF Model in lieu of the observed z_0.

hurricanes in WRF. A total of 10 category-1–5 hurricanes are simulated using WRF with four momentum roughness length formulations. In one set of these simulations, the ocean surface wave is explicitly resolved by coupling WRF with the SWAN model in the framework of COAWST to account for wave-induced drag. A total of 310 simulations of a wide range of hurricane cases were conducted by varying the parameter space of the WRF system (e.g., PBL schemes, and surface flux options). The key findings of this study are summarized as follows:

(i) Among all the default models and PBL schemes considered, WRF-YSU-1 overall provided the most accurate hurricane intensity prediction (e.g., ~14% average improved intensity forecasts compared to the MYJ scheme), while WRF-COAWST yielded the best track forecasts in the 10 considered hurricanes (≳8% improvement on average compared to MYJ and YSU schemes).

(ii) The momentum roughness length significantly influenced the hurricane track and intensity simulations. Decreasing the default z_0 intensified the hurricanes and remarkably increased their maximum surface wind intensity. Momentum budget analysis showed that for the same pressure gradient force, decreasing z_0 decreases the friction and in turn increases the maximum near surface wind speed.

(iii) For the considered category-3–5 hurricanes, the accuracy of track and intensity forecasts was greatly improved by decreasing the momentum roughness length, however, such improvement was not observed in the simulations of category-1–2 hurricanes. For all model configurations, ~24% (~32%) improvement was observed on average for intensity predictions when using Clz = 0.01 (Clz = 0.0001), and ~12% (~6%) improvement was obtained on average for track forecasts compared to the default roughness length parameterization. We showed that decreasing the default z_0 generally increased the size of the considered hurricanes, but more observational data and analysis are needed to confirm if this change improves the spatial structure and asymmetry of hurricanes compared to observations.

(iv) The C_k/C_d ratio was increased in Clz = 0.01 (Clz = 0.0001) cases to 1.2 ± 0.1 (1.7 ± 0.1) from the default value of 0.8 ± 0.1. The values of this ratio in the reduced z_0 cases fall in the high wind regions range of intense storms (~1.2–1.5) that is predicted by the MPI theory. The positive correlation between the storm intensity and this ratio in our simulations of strong hurricanes is consistent with the MPI theory finding.

(v) WRF's default z_0 values were compared with the estimates using a large sample of GPS dropsonde data, showing agreement in weak hurricanes but an overestimation of z_0 in strong hurricanes. This mismatch at large wind speeds between WRF and observations further explains the poor performance of the default z_0 parameterization for strong hurricane forecasts. Hence, our results suggested decreasing the default z_0 values in WRF in high surface wind conditions ($U_{10} \gtrsim 45$ m s^{-1}) to improve their intensity predictions.

This study provides insights into the role of surface momentum fluxes in real hurricane simulations. The findings may be useful for improving operational weather and climate models to enhance hurricane forecasts.

Acknowledgments. The authors acknowledge support from the Department of Civil and Environmental Engineering at the University of Houston via startup funds, as well as the Physical and Dynamic Meteorology Program of the National Science Foundation under Grant AGS-2228299. This project has also been funded partially with funds from the State of Texas as part of the program of the Texas Air Research Center (TARC) Grant 012UHH0198A. The contents do not necessarily reflect the views and policies of the sponsor nor does the mention of trade names or commercial products constitute endorsement or recommendation for use. The simulations were performed on the University of Houston's computing clusters (Carya and Sabine). Jun A. Zhang was supported by Office of Naval Research Grant N00014-20-1-2071 and NOAA Grant NA21OAR4590370.

Data availability statement. The data for the observed best tracks and the dropsondes are already presented in the paper. The data for two hurricane simulation outputs (one strong and one weak) that include 3D snapshots of the velocity field, pressure, and temperature in NetCDF format can be found in Li et al. (2023). The readers can access some of the simulation data of this paper and an instruction to load them via Python codes in this repository.

REFERENCES

Abarca, S., and K. Corbosiero, 2011: Secondary eyewall formation in WRF simulations of Hurricanes Rita and Katrina (2005).

Geophys. Res. Lett., **38**, L07802, https://doi.org/10.1029/2011GL047015.

Alimohammadi, M., H. Malakooti, and M. Rahbani, 2020: Comparison of momentum roughness lengths of the WRF-SWAN online coupling and WRF model in simulation of tropical cyclone Gonu. *Ocean Dyn.*, **70**, 1531–1545, https://doi.org/10.1007/s10236-020-01417-w.

Andreas, E. L, and K. A. Emanuel, 2001: Effects of sea spray on tropical cyclone intensity. *J. Atmos. Sci.*, **58**, 3741–3751, https://doi.org/10.1175/1520-0469(2001)058<3741:EOSSOT>2.0.CO;2.

Bjarnadottir, S., Y. Li, and M. G. Stewart, 2011: A probabilistic-based framework for impact and adaptation assessment of climate change on hurricane damage risks and costs. *Struct. Saf.*, **33**, 173–185, https://doi.org/10.1016/j.strusafe.2011.02.003.

Blake, B. T., D. B. Parsons, K. R. Haghi, and S. G. Castleberry, 2017: The structure, evolution, and dynamics of a nocturnal convective system simulated using the WRF-ARW Model. *Mon. Wea. Rev.*, **145**, 3179–3201, https://doi.org/10.1175/MWR-D-16-0360.1.

Blake, E. S., E. N. Rappaport, and C. W. Landsea, 2007: The deadliest, costliest, and most intense United States tropical cyclones from 1851 to 2006 (and other frequently requested hurricane facts). NOAA Tech. Memo. NWS TPC-5, 45 pp., https://www.nhc.noaa.gov/pdf/NWS-TPC-5.pdf.

Bryan, G. H., R. P. Worsnop, J. K. Lundquist, and J. A. Zhang, 2017: A simple method for simulating wind profiles in the boundary layer of tropical cyclones. *Bound.-Layer Meteor.*, **162**, 475–502, https://doi.org/10.1007/s10546-016-0207-0.

Cavallo, S., R. Torn, C. Snyder, C. Davis, W. Wang, and J. Done, 2013: Evaluation of the Advanced Hurricane WRF data assimilation system for the 2009 Atlantic hurricane season. *Mon. Wea. Rev.*, **141**, 523–541, https://doi.org/10.1175/MWR-D-12-00139.1.

Cheikh, M. I., and M. Momen, 2020: The interacting effects of storm surge intensification and sea-level rise on coastal resiliency: A high-resolution turbulence resolving case study. *Environ. Res. Commun.*, **2**, 115002, https://doi.org/10.1088/2515-7620/abc39e.

Chen, S. S., J. F. Price, W. Zhao, M. A. Donelan, and E. J. Walsh, 2007: The CBLAST-Hurricane program and the next-generation fully coupled atmosphere–wave–ocean models for hurricane research and prediction. *Bull. Amer. Meteor. Soc.*, **88**, 311–317, https://doi.org/10.1175/BAMS-88-3-311.

——, W. Zhao, M. A. Donelan, and H. L. Tolman, 2013: Directional wind–wave coupling in fully coupled atmosphere–wave–ocean models: Results from CBLAST-Hurricane. *J. Atmos. Sci.*, **70**, 3198–3215, https://doi.org/10.1175/JAS-D-12-0157.1.

Chen, X., 2022: How do planetary boundary layer schemes perform in hurricane conditions: A comparison with large-eddy simulations. *J. Adv. Model. Earth Syst.*, **14**, e2022MS003088, https://doi.org/10.1029/2022MS003088.

——, G. H. Bryan, J. A. Zhang, J. J. Cione, and F. D. Marks, 2021: A framework for simulating the tropical cyclone boundary layer using large-eddy simulation and its use in evaluating PBL parameterizations. *J. Atmos. Sci.*, **78**, 3559–3574, https://doi.org/10.1175/JAS-D-20-0227.1.

——, ——, A. Hazelton, F. D. Marks, and P. Fitzpatrick, 2022: Evaluation and improvement of a TKE-based eddy-diffusivity mass-flux (EDMF) planetary boundary layer scheme in hurricane conditions. *Wea. Forecasting*, **37**, 935–951, https://doi.org/10.1175/WAF-D-21-0168.1.

Curcic, M., and B. K. Haus, 2020: Revised estimates of ocean surface drag in strong winds. *Geophys. Res. Lett.*, **47**, e2020GL087647, https://doi.org/10.1029/2020GL087647.

Davis, C., and Coauthors, 2008: Prediction of landfalling hurricanes with the Advanced Hurricane WRF Model. *Mon. Wea. Rev.*, **136**, 1990–2005, https://doi.org/10.1175/2007MWR2085.1.

Di, Z., and Coauthors, 2015: Assessing WRF model parameter sensitivity: A case study with 5 day summer precipitation forecasting in the Greater Beijing Area. *Geophys. Res. Lett.*, **42**, 579–587, https://doi.org/10.1002/2014GL061623.

Dietrich, J. C., and Coauthors, 2011: Modeling hurricane waves and storm surge using integrally-coupled, scalable computations. *Coast. Eng.*, **58**, 45–65, https://doi.org/10.1016/j.coastaleng.2010.08.001.

Donelan, M. A., B. K. Haus, N. Reul, W. J. Plant, M. Stiassnie, H. C. Graber, O. B. Brown, and E. S. Saltzman, 2004: On the limiting aerodynamic roughness of the ocean in very strong winds. *Geophys. Res. Lett.*, **31**, L18306, https://doi.org/10.1029/2004GL019460.

Emanuel, K. A., 2003: A similarity hypothesis for air–sea exchange at extreme wind speeds. *J. Atmos. Sci.*, **60**, 1420–1428, https://doi.org/10.1175/1520-0469(2003)060<1420:ASHFAE>2.0.CO;2.

——, 1988: The maximum intensity of hurricanes. *J. Atmos. Sci.*, **45**, 1143–1155, https://doi.org/10.1175/1520-0469(1988)045<1143:TMIOH>2.0.CO;2.

——, 1995: Sensitivity of tropical cyclones to surface exchange coefficients and a revised steady-state model incorporating eye dynamics. *J. Atmos. Sci.*, **52**, 3969–3976, https://doi.org/10.1175/1520-0469(1995)052<3969:SOTCTS>2.0.CO;2.

——, 2005: Increasing destructiveness of tropical cyclones over the past 30 years. *Nature*, **436**, 686–688, https://doi.org/10.1038/nature03906.

——, 2020: Evidence that hurricanes are getting stronger. *Proc. Natl. Acad. Sci. USA*, **117**, 13 194–13 195, https://doi.org/10.1073/pnas.2007742117.

Fierro, A. O., R. F. Rogers, F. D. Marks, and D. S. Nolan, 2009: The impact of horizontal grid spacing on the microphysical and kinematic structures of strong tropical cyclones simulated with the WRF-ARW Model. *Mon. Wea. Rev.*, **137**, 3717–3743, https://doi.org/10.1175/2009MWR2946.1.

French, J. R., W. M. Drennan, J. A. Zhang, and P. G. Black, 2007: Turbulent fluxes in the hurricane boundary layer. Part I: Momentum flux. *J. Atmos. Sci.*, **64**, 1089–1102, https://doi.org/10.1175/JAS3887.1.

Gopalakrishnan, S. G., F. Marks, J. A. Zhang, X. Zhang, J. W. Bao, and V. Tallapragada, 2013: A study of the impacts of vertical diffusion on the structure and intensity of the tropical cyclones using the high-resolution HWRF system. *J. Atmos. Sci.*, **70**, 524–541, https://doi.org/10.1175/JAS-D-11-0340.1.

——, A. Hazelton, and J. A. Zhang, 2021: Improving hurricane boundary layer parameterization scheme based on observations. *Earth Space Sci.*, **8**, e2020EA001422, https://doi.org/10.1029/2020EA001422.

Green, B. W., and F. Zhang, 2013: Impacts of air–sea flux parameterizations on the intensity and structure of tropical cyclones. *Mon. Wea. Rev.*, **141**, 2308–2324, https://doi.org/10.1175/MWR-D-12-00274.1.

——, and ——, 2014: Sensitivity of tropical cyclone simulations to parametric uncertainties in air–sea fluxes and implications for parameter estimation. *Mon. Wea. Rev.*, **142**, 2290–2308, https://doi.org/10.1175/MWR-D-13-00208.1.

Hazelton, A., J. A. Zhang, and S. Gopalakrishnan, 2022: Comparison of the performance of the observation-based hybrid EDMF and EDMF-TKE PBL schemes in 2020 tropical cyclone forecasts from the Global-Nested Hurricane Analysis and Forecast System. *Wea. Forecasting*, **37**, 457–476, https://doi.org/10.1175/WAF-D-21-0124.1.

Holthuijsen, L. H., M. D. Powell, and J. D. Pietrzak, 2012: Wind and waves in extreme hurricanes. *J. Geophys. Res.*, **117**, C09003, https://doi.org/10.1029/2012JC007983.

Hong, S.-Y., 2010: A new stable boundary-layer mixing scheme and its impact on the simulated East Asian summer monsoon. *Quart. J. Roy. Meteor. Soc.*, **136**, 1481–1496, https://doi.org/10.1002/qj.665.

——, Y. Noh, and J. Dudhia, 2006: A new vertical diffusion package with an explicit treatment of entrainment processes. *Mon. Wea. Rev.*, **134**, 2318–2341, https://doi.org/10.1175/MWR3199.1.

Hosannah, N., P. Ramamurthy, J. Marti, J. Munoz, and J. E. González, 2021: Impacts of Hurricane Maria on land and convection modification over Puerto Rico. *J. Geophys. Res. Atmos.*, **126**, e2020JD032493, https://doi.org/10.1029/2020JD032493.

Huang, Y., R. H. Weisberg, L. Zheng, and M. Zijlema, 2013: Gulf of Mexico hurricane wave simulations using SWAN: Bulk formula-based drag coefficient sensitivity for Hurricane Ike. *J. Geophys. Res. Oceans*, **118**, 3916–3938, https://doi.org/10.1002/jgrc.20283.

Huffman, G. J., D. T. Bolvin, D. Braithwaite, K. Hsu, R. Joyce, P. Xie, and S.-H. Yoo, 2015: NASA Global Precipitation Measurement (GPM) Integrated Multi-SatellitE Retrievals for GPM (IMERG). Algorithm Theoretical Basis Doc., version 4.26, 26 pp.

Janjić, Z. I., 1990: The step-mountain coordinate: Physical package. *Mon. Wea. Rev.*, **118**, 1429–1443. https://doi.org/10.1175/1520-0493(1990)118<1429:TSMCPP>2.0.CO;2

——, 1994: The step-mountain eta coordinate model: Further developments of the convection, viscous sublayer, and turbulence closure schemes. *Mon. Wea. Rev.*, **122**, 927–945, https://doi.org/10.1175/1520-0493(1994)122<0927:TSMECM>2.0.CO;2.

Katsafados, P., G. Varlas, A. Papadopoulos, C. Spyrou, and G. Korres, 2018: Assessing the implicit rain impact on sea state during Hurricane Sandy (2012). *Geophys. Res. Lett.*, **45**, 12–15, https://doi.org/10.1029/2018GL078673.

Khain, A., B. Lynn, and J. Shpund, 2016: High resolution WRF simulations of Hurricane Irene: Sensitivity to aerosols and choice of microphysical schemes. *Atmos. Res.*, **167**, 129–145, https://doi.org/10.1016/j.atmosres.2015.07.014.

Kidder, S. Q., M. D. Goldberg, R. M. Zehr, M. DeMaria, J. F. W. Purdom, C. S. Velden, N. C. Grody, and S. J. Kusselson, 2000: Satellite analysis of tropical cyclones using the Advanced Microwave Sounding Unit (AMSU). *Bull. Amer. Meteor. Soc.*, **81**, 1241–1260, https://doi.org/10.1175/1520-0477(2000)081<1241:SAOTCU>2.3.CO;2.

Klotz, B. W., and E. W. Uhlhorn, 2014: Improved stepped frequency microwave radiometer tropical cyclone surface winds in heavy precipitation. *J. Atmos. Oceanic Technol.*, **31**, 2392–2408, https://doi.org/10.1175/JTECH-D-14-00028.1.

Kousky, C., 2014: Informing climate adaptation: A review of the economic costs of natural disasters. *Energy Econ.*, **46**, 576–592, https://doi.org/10.1016/j.eneco.2013.09.029.

Large, W. G., and S. Pond, 1981: Open ocean momentum flux measurements in moderate to strong winds. *J. Phys. Oceanogr.*, **11**, 324–336, https://doi.org/10.1175/1520-0485(1981)011<0324:OOMFMI>2.0.CO;2.

Li, M., Z. Zhao, Y. Pandya, G. V. Iungo, and D. Yang, 2019: Large-eddy simulations of oil droplet aerosol transport in the marine atmospheric boundary layer. *Atmosphere*, **10**, 459, https://doi.org/10.3390/atmos10080459.

——, J. A. Zhang, L. Matak, and M. Momen, 2023: The impacts of adjusting momentum roughness length on strong and weak hurricanes forecasts: A comprehensive analysis of weather simulations and observations. Harvard dataverse, version 1, https://doi.org/10.7910/DVN/A1CNOJ.

Lyu, H., and J. Zhu, 2018: Impact of the bottom drag coefficient on saltwater intrusion in the extremely shallow estuary. *J. Hydrol.*, **557**, 838–850, https://doi.org/10.1016/j.jhydrol.2018.01.010.

Mellor, G. L., and T. Yamada, 1982: Development of a turbulence closure model for geophysical fluid problems. *Rev. Geophys.*, **20**, 851–875, https://doi.org/10.1029/RG020i004p00851.

Miller, B. I., 1964: A study of the filling of Hurricane Donna (1960) over land. *Mon. Wea. Rev.*, **92**, 389–406, https://doi.org/10.1175/1520-0493(1964)092<0389:ASOTFO>2.3.CO;2.

Momen, M., 2022: Baroclinicity in stable atmospheric boundary layers: Characterizing turbulence structures and collapsing wind profiles via reduced models and large-eddy simulations. *Quart. J. Roy. Meteor. Soc.*, **148**, 76–96, https://doi.org/10.1002/qj.4193.

——, and E. Bou-Zeid, 2016: Large-eddy simulations and damped-oscillator models of the unsteady Ekman boundary layer. *J. Atmos. Sci.*, **73**, 25–40, https://doi.org/10.1175/JAS-D-15-0038.1.

——, ——, M. B. Parlange, and M. Giometto, 2018: Modulation of mean wind and turbulence in the atmospheric boundary layer by baroclinicity. *J. Atmos. Sci.*, **75**, 3797–3821, https://doi.org/10.1175/JAS-D-18-0159.1.

——, M. B. Parlange, and M. G. Giometto, 2021: Scrambling and reorientation of classical atmospheric boundary layer turbulence in hurricane winds. *Geophys. Res. Lett.*, **48**, e2020GL091695, https://doi.org/10.1029/2020GL091695.

Montgomery, M. T., G. L. Thomsen, and R. K. Smith, 2011: Sensitivity of tropical-cyclone models to the surface drag coefficient in different boundary-layer schemes. *Quart. J. Roy. Meteor. Soc.*, **140**, 792–804, https://doi.org/10.1002/qj.2057.

Moon, I.-J., I. Ginis, and T. Hara, 2004: Effect of surface waves on air–sea momentum exchange. Part II: Behavior of drag coefficient under tropical cyclones. *J. Atmos. Sci.*, **61**, 2334–2348, https://doi.org/10.1175/1520-0469(2004)061<2334:EOSWOA>2.0.CO;2.

Mooney, P. A., F. J. Mulligan, C. L. Bruyère, C. L. Parker, and D. O. Gill, 2019: Investigating the performance of coupled WRF-ROMS simulations of Hurricane Irene (2011) in a regional climate modeling framework. *Atmos. Res.*, **215**, 57–74, https://doi.org/10.1016/j.atmosres.2018.08.017.

Nasrollahi, N., A. AghaKouchak, J. Li, X. Gao, K. Hsu, and S. Sorooshian, 2012: Assessing the impacts of different WRF precipitation physics in hurricane simulations. *Wea. Forecasting*, **27**, 1003–1016, https://doi.org/10.1175/WAF-D-10-05000.1.

NCEP/NWS/NOAA/U.S. Department of Commerce, 2015: NCEP GFS 0.25 degree global forecast grids historical archive. Research Data Archive at the National Center for Atmospheric Research, Computational and Information Systems Laboratory, accessed 16 January 2023, https://doi.org/10.5065/D65D8PWK.

Nellipudi, N. R., Y. Viswanadhapalli, V. S. Challa, N. K. Vissa, and S. Langodan, 2021: Impact of surface roughness parameterizations on tropical cyclone simulations over the Bay of

Bengal using WRF-OML model. *Atmos. Res.*, **262**, 105779, https://doi.org/10.1016/j.atmosres.2021.105779.

NOAA/NCEI, 2021: U.S. billion-dollar weather and climate disasters. NOAA/NCEI, accessed 16 January 2023, https://doi.org/10.25921/stkw-7w73, https://www.ncei.noaa.gov/access/billions/.

Nolan, D. S., J. A. Zhang, and D. P. Stern, 2009: Evaluation of planetary boundary layer parameterizations in tropical cyclones by comparison of in situ observations and high-resolution simulations of Hurricane Isabel (2003). Part I: Initialization, maximum winds, and the outer-core boundary layer. *Mon. Wea. Rev.*, **137**, 3651–3674, https://doi.org/10.1175/2009MWR2785.1.

O'Brien, J. J., 1970: A note on the vertical structure of the eddy exchange coefficient in the planetary boundary layer. *J. Atmos. Sci.*, **27**, 1213–1215, https://doi.org/10.1175/1520-0469(1970)027<1213:ANOTVS>2.0.CO;2.

Phibbs, S., and R. Toumi, 2014: Modeled dependence of wind and waves on ocean temperature in tropical cyclones. *Geophys. Res. Lett.*, **41**, 7383–7390, https://doi.org/10.1002/2014GL061721.

Pielke, R. A., Jr., J. Gratz, C. W. Landsea, D. Collins, M. A. Saunders, and R. Musulin, 2008: Normalized hurricane damage in the United States: 1900–2005. *Nat. Hazards Rev.*, **9**, 29–42, https://doi.org/10.1061/(ASCE)1527-6988(2008)9:1(29).

Pinelli, J.-P., E. Simiu, K. Gurley, C. Subramanian, L. Zhang, A. Cope, J. J. Filliben, and S. Hamid, 2004: Hurricane damage prediction model for residential structures. *J. Struct. Eng.*, **130**, 1685–1691, https://doi.org/10.1061/(ASCE)0733-9445(2004)130:11(1685).

Powell, M. D., and I. Ginis, 2006: Drag coefficient distribution and wind speed dependence in tropical cyclones. Final Report to the National Oceanic and Atmospheric Administration (NOAA) Joint Hurricane Testbed (JHT) Program, 26 pp., https://www.nhc.noaa.gov/jht/05-07reports/final_Powell_JHT07.pdf.

——, P. J. Vickery, and T. A. Reinhold, 2003: Reduced drag coefficient for high wind speeds in tropical cyclones. *Nature*, **422**, 279–283, https://doi.org/10.1038/nature01481.

Richter, D. H., C. Wainwright, D. P. Stern, G. H. Bryan, and D. Chavas, 2021: Potential low bias in high-wind drag coefficient inferred from dropsonde data in hurricanes. *J. Atmos. Sci.*, **78**, 2339–2352, https://doi.org/10.1175/JAS-D-20-0390.1.

Romdhani, O., J. A. Zhang, and M. Momen, 2022: Characterizing the impacts of turbulence closures on real hurricane forecasts: A comprehensive joint assessment of grid resolution, horizontal turbulence models, and horizontal mixing length. *J. Adv. Model. Earth Syst.*, **14**, e2021MS002796, https://doi.org/10.1029/2021MS002796.

Salesky, S. T., M. Chamecki, and E. Bou-Zeid, 2016: On the nature of the transition between roll and cellular organization in the convective boundary layer. *Bound.-Layer Meteor.*, **163**, 41–68, https://doi.org/10.1007/s10546-016-0220-3.

Sheng, Y. P., Y. Zhang, and V. A. Paramygin, 2010: Simulation of storm surge, wave, and coastal inundation in the Northeastern Gulf of Mexico region during Hurricane Ivan in 2004. *Ocean Modell.*, **35**, 314–331, https://doi.org/10.1016/j.ocemod.2010.09.004.

Simpson, R. H., and H. Saffir, 1974: The hurricane disaster potential scale. *Weatherwise*, **27**, 169–186, https://doi.org/10.1080/00431672.1974.9931702.

Skamarock, W. C., and Coauthors, 2008: A description of the Advanced Research WRF version 3. NCAR Tech. Note NCAR/TN-475+STR, 113 pp., https://doi.org/10.5065/D68S4MVH.

Stewart, M. G., D. V. Rosowsky, and Z. Huang, 2003: Hurricane risks and economic viability of strengthened construction. *Nat. Hazards Rev.*, **4**, 12–19, https://doi.org/10.1061/(ASCE)1527-6988(2003)4:1(12).

Stull, R., 1988: *An Introduction to Boundary Layer Meteorology*. Kluwer Academic, 666 pp.

Taylor, H. T., B. Ward, M. Willis, and W. Zaleski, 2010: The Saffir-Simpson Hurricane Wind Scale. NOAA, 4 pp., https://www.nhc.noaa.gov/pdf/sshws.pdf.

Taylor, P. K., and M. J. Yelland, 2001: The dependence of sea surface roughness on the height and steepness of the waves. *J. Phys. Oceanogr.*, **31**, 572–590, https://doi.org/10.1175/1520-0485(2001)031<0572:TDOSSR>2.0.CO;2.

Warner, J. C., N. Perlin, and E. D. Skyllingstad, 2008: Using the Model Coupling Toolkit to couple earth system models. *Environ. Modell. Software*, **23**, 1240–1249, https://doi.org/10.1016/j.envsoft.2008.03.002.

——, B. Armstrong, R. He, and J. B. Zambon, 2010: Development of a coupled ocean–atmosphere–wave–sediment transport (COAWST) modeling system. *Ocean Modell.*, **35**, 230–244, https://doi.org/10.1016/j.ocemod.2010.07.010.

Wei, W., and Coauthors, 2019: WRF ARW version 4 modeling system user's guide. UCAR, 464 pp., https://www2.mmm.ucar.edu/wrf/users/docs/user_guide_v4/v4.2/WRFUsersGuide_v42.pdf.

Xie, L., H. Liu, and M. Peng, 2008: The effect of wave–current interactions on the storm surge and inundation in Charleston Harbor during Hurricane Hugo 1989. *Ocean Modell.*, **20**, 252–269, https://doi.org/10.1016/j.ocemod.2007.10.001.

Xu, F., W. Perrie, B. Toulany, and P. C. Smith, 2007: Wind-generated waves in Hurricane Juan. *Ocean Modell.*, **16**, 188–205, https://doi.org/10.1016/j.ocemod.2006.09.001.

Xu, L., H. Liu, Q. Du, and L. Wang, 2016: Evaluation of the WRF-lake model over a highland freshwater lake in southwest China. *J. Geophys. Res. Atmos.*, **121**, 13 989–14 005, https://doi.org/10.1002/2016JD025396.

Zhang, J. A., 2010: Spectral characteristics of turbulence in the hurricane boundary layer over the ocean between the outer rain bands. *Quart. J. Roy. Meteor. Soc.*, **136**, 918–926, https://doi.org/10.1002/qj.610.

——, W. M. Drennan, P. G. Black, and J. R. French, 2009: Turbulence structure of the hurricane boundary layer between the outer rainbands. *J. Atmos. Sci.*, **66**, 2455–2467, https://doi.org/10.1175/2009JAS2954.1.

——, R. F. Rogers, D. S. Nolan, and F. D. Marks Jr., 2011: On the characteristic height scales of the hurricane boundary layer. *Mon. Wea. Rev.*, **139**, 2523–2535, https://doi.org/10.1175/MWR-D-10-05017.1.

——, ——, and V. Tallapragada, 2017: Impact of parameterized boundary layer structure on tropical cyclone rapid intensification forecasts in HWRF. *Mon. Wea. Rev.*, **145**, 1413–1426, https://doi.org/10.1175/MWR-D-16-0129.1.